

Design and FPGA implementation of multi-wing chaotic switched systems based on a quadratic transformation

Qing-Yu Shi(石擎宇), Xia Huang(黄霞)†, Fang Yuan(袁方), and Yu-Xia Li(李玉霞)
Citation: Chin. Phys. B, 2021, 30 (**2**): 020507. DOI: 10.1088/1674-1056/abd74c
Journal homepage: http://cpb.iphy.ac.cn; http://iopscience.iop.org/cpb

What follows is a list of articles you may be interested in

A multi-directional controllable multi-scroll conservative chaos generator: Modelling, analysis, and FPGA implementation

En-Zeng Dong(董恩增), Rong-Hao Li(李荣昊), and Sheng-Zhi Du(杜升之)
Chin. Phys. B, 2021, 30 (**2**): 020505. DOI: 10.1088/1674-1056/abc239

Chaotic signal denoising algorithm based on sparse decomposition

Jin-Wang Huang(黄锦旺), Shan-Xiang Lv(吕善翔), Zu-Sheng Zhang(张足生), Hua-Qiang Yuan(袁华强)
Chin. Phys. B, 2020, 29 (**6**): 060505. DOI: 10.1088/1674-1056/ab8a3b

Hidden attractors in a new fractional-order discrete system: Chaos, complexity, entropy, and control

Adel Ouannas, Amina Aicha Khennaoui, Shaher Momani, Viet-Thanh Pham, Reyad El-Khazali
Chin. Phys. B, 2020, 29 (**5**): 050504. DOI: 10.1088/1674-1056/ab820d

Topological horseshoe analysis and field-programmable gate array implementation of a fractional-order four-wing chaotic attractor

En-Zeng Dong(董恩增), Zhen Wang(王震), Xiao Yu(于晓), Zeng-Qiang Chen(陈增强), Zeng-Hui Wang(王增会)
Chin. Phys. B, 2018, 27 (**1**): 010503. DOI: 10.1088/1674-1056/27/1/010503

Study on a new chaotic bitwise dynamical system and its FPGA implementation

Wang Qian-Xue, Yu Si-Min, C. Guyeux, J. Bahi, Fang Xiao-Le
Chin. Phys. B, 2015, 24 (**6**): 060503. DOI: 10.1088/1674-1056/24/6/060503

Design and FPGA implementation of multi-wing chaotic switched systems based on a quadratic transformation*

Qing-Yu Shi(石擎宇), Xia Huang(黄霞)†, Fang Yuan(袁方), and Yu-Xia Li(李玉霞)

College of Electrical Engineering and Automation, Shandong University of Science and Technology, Qingdao 266590, China

(Received 12 October 2020; revised manuscript received 23 December 2020; accepted manuscript online 30 December 2020)

Based on a quadratic transformation and a switching function, a novel multi-wing chaotic switched system is proposed. First, a 4-wing chaotic system is constructed from a 2-wing chaotic system on the basis of a quadratic transformation. Then, a switching function is designed and by adjusting the switching function, the number and the distribution of the saddle-focus equilibrium points of the switched system can be regulated. Thus, a set of chaotic switched systems, which can produce 6-to-8-12-16-wing attractors, are generated. The Lyapunov exponent spectra, bifurcation diagrams, and Poincaré maps are given to verify the existence of the chaotic attractors. Besides, the digital circuit of the multi-wing chaotic switched system is designed by using the Verilog HDL fixed-point algorithm and the state machine control. Finally, the multi-wing chaotic attractors are demonstrated via FPGA platform. The experimental results show that the number of the wings of the chaotic attractors can be expanded more effectively with the combination of the quadratic transformation and the switching function methods.

Keywords: quadratic transformation, chaotic switched system, FPGA

PACS: 05.45.−a **DOI:** 10.1088/1674-1056/abd74c

1. Introduction

At present, design and implementation of multi-wing or multi-scroll chaotic systems with rich dynamic properties on the basis of chaos and circuit theory have become an important research topic.[1–10] The research on the generation of multi-scroll chaotic systems has been relatively mature, but it is still challenging to design the multi-wing chaotic systems. Compared with conventional 2-wing chaotic systems, multi-wing chaotic systems not only have more key parameters, but also have nested topological structures.[11–14] They show their unique advantages in relevant fields such as information security and secret communication.[15–18]

In recent decades, a large number of scholars at home and abroad have been devoted to the generation and realization of multi-wing chaotic attractors. For example, Lin *et al.* constructed a multi-wing chaotic system by introducing the sawtooth wave function to the Lorenz system.[19] Huang *et al.* proposed a new four-dimensional chaotic system based on Sprott B chaotic system, which can produce not only 2-wing and 4-wing attractors, but also symmetric coexisting attractors.[20] Zhang *et al.* developed a novel method of constructing multi-wing chaotic and hyperchaotic systems by using a unified step function.[21] Chang *et al.* presented a novel memristor-based chaotic system, and the implemented chaotic attractors had a 2×3-wing, 2×2-wing, and 2×1-wing.[22] Zhong *et al.* employed a second-degree polynomial memristor function and a sixth-order exponent internal state memristor function to design a three-dimensional memristor-based chaotic system, which formed 2-to-8-wing chaotic attractors.[23] From the above analysis, it is easy to find that most of the literature concentrated on using a particular kind of nonsmooth functions (e.g., piecewise linear functions, sine functions, stair functions, and saturated functions) or using memristor devices to expand the number of wings. To increase the number of wings rapidly, this paper is devoted to combining the switching function method with the state transformation method to produce a series of multi-wing chaotic attractors.

On the other hand, the research on multi-wing chaotic systems is no longer limited to theoretical analysis and numerical simulations but includes analog or digital circuits realization.[24–29] In actual analog circuits, strict requirements are usually placed on the electronic components, and therefore many factors such as the aging of the devices and the interference of the external environments have a dramatic impact on the dynamics of the considered system. However, the use of field programmable gate array (FPGA) digital systems can well avoid these problems. In regard to FPGA implementation, there are usually three methods. The first is to use the Verilog HDL or HDL code directly to describe the chaotic system.[30–32] The advantage of this method is that the codes have good portability and versatility, but the programming is quite complicated. The second is to use the DSP Builder to construct a discrete model for the considered chaotic system and then output HDL codes.[33,34] This method adopts graphical programming, and hence the code is relatively simple to

*Project supported by the National Natural Science Foundation of China (Grant Nos. 61973199 and 61973200) and the Taishan Scholar Project of Shandong Province of China.

†Corresponding author. E-mail: huangxia_qd@126.com

© 2021 Chinese Physical Society and IOP Publishing Ltd

write, but the portability is low. The third is to use the HDL Coder to generate Verilog HDL or HDL code in the Matlab/Simulink environment.[35,36] This method combines the advantages of the first and the second, but the library functions are still not perfect, and some computing functions are difficult to implement. With careful consideration of these three methods, the Verilog HDL code is used directly to describe the state equations of the considered system. We convert the generated digital chaotic sequence into an analog voltage signal by the digital-to-analog converter (DAC) module, and then the phase diagrams of the chaotic attractors can be observed on the oscilloscope.

In summary, we propose a combined method in this paper to generate multi-wing chaotic attractors. More precisely, we combine the quadratic transformation with a switching function to expand the number of saddle-focus equilibrium points, and meanwhile the FPGA is built to confirm the numerically simulations.

Comparing with the existing literature, the innovations of this paper are as follows.

(1) Most of the published literature used only one method to expand the number of wings, while this paper combines two different techniques to generate the multi-wing chaotic attractors. The proposed system can produce 6-to-8-12-16-wing attractors by adjusting the switching function and it makes the generation of multi-wing chaotic attractors easier.

(2) Most of the chaotic attractors in the published literature are arranged in linear or grid form. In contrast, the chaotic attractors generated in this paper are distributed in a fish-bone like structure, and the topological structures are more complicated.

(3) In FPGA implementation, we use the three-stage state machine design to write Verilog HDL code directly to realize the chaotic switched systems. Compared with the existing work, there exist more difficulties in the FPGA design.

The rest of the paper is organized as follows. In Section 2, by using the quadratic transformation scheme, the state variables of a 2-wing chaotic system are transformed into another group of state variables to generate a 4-wing chaotic attractor, and it is shown that the number of wings is equal to the number of the saddle-focus equilibrium points. In Section 3, the number of the saddle-focus equilibrium points is increased by constructing a kind of switching functions. Thus, the previously generated 4-wing chaotic attractor can be transformed into a series of attractors with 6-to-8-12-16 wings, which are also testified by the Lyapunov exponent spectra, Poincaré maps, and bifurcation diagrams. In Section 4, the Verilog HDL code for the multi-wing switched chaotic system is designed. By using FPGA, the chaotic attractors are observed on the oscilloscope, which verifies the feasibility of our design method.

2. A four-wing chaotic system based on the quadratic transformation

Consider a three-dimensional 2-wing chaotic system[37] as follows:

$$\begin{bmatrix} \dot{u} \\ \dot{v} \\ \dot{w} \end{bmatrix} = \begin{bmatrix} -a_1 u + vw \\ -u + a_2 v \\ -a_3 w + a_4 v^2 \end{bmatrix}, \tag{1}$$

where u, v, w are the state variables, and a_1, a_2, a_3, a_4 are the system parameters.

First, the quadratic transformation[38] is applied to system (1). The specific steps are as follows.

Step 1: Denote the space transformation as $\Phi_0 = x + y\mathrm{i}$, where Φ_0 is a complex number with x and y as its real and imaginary parts. Introduce the quadratic transformation Φ_1 as follows:

$$\Phi_1 = \Phi_0^2 = (x^2 - y^2) + 2xy\mathrm{i}, \tag{2}$$

where $(x^2 - y^2)$ is the real part of Φ_1, and $2xy$ is the imaginary part of Φ_1.

Step 2: Let the state variables u and v be the real and imaginary part of Φ_1, respectively. And, the state variable w is replaced by a new variable z, that is

$$u = x^2 - y^2, \quad v = 2xy, \quad w = z. \tag{3}$$

Step 3: In view of Eq. (3), the relations between the state variables u, v, w and x, y, z can be represented by

$$\begin{bmatrix} \dot{u} \\ \dot{v} \\ \dot{w} \end{bmatrix} = \begin{bmatrix} 2x & -2y & 0 \\ 2y & 2x & 0 \\ 0 & 0 & 1 \end{bmatrix} \begin{bmatrix} \dot{x} \\ \dot{y} \\ \dot{z} \end{bmatrix}. \tag{4}$$

Step 4: By the matrix inverse algorithm, equation (4) can be further rewritten as

$$\begin{bmatrix} \dot{x} \\ \dot{y} \\ \dot{z} \end{bmatrix} = \frac{1}{4x^2 + 4y^2} \begin{bmatrix} 2x & 2y & 0 \\ -2y & 2x & 0 \\ 0 & 0 & 4x^2 + 4y^2 \end{bmatrix} \begin{bmatrix} \dot{u} \\ \dot{v} \\ \dot{w} \end{bmatrix}, \tag{5}$$

which is equivalent to

$$\begin{bmatrix} \dot{x} \\ \dot{y} \\ \dot{z} \end{bmatrix} = \frac{1}{4x^2 + 4y^2} \begin{bmatrix} 2x & 2y & 0 \\ -2y & 2x & 0 \\ 0 & 0 & 4x^2 + 4y^2 \end{bmatrix} \times \begin{bmatrix} -a_1(x^2 - y^2) + (2xy)z \\ -(x^2 - y^2) + a_2(2xy) \\ -a_3 z + a_4(2xy)^2 \end{bmatrix}. \tag{6}$$

Thus, based on the quadratic transformation, system (1) is transformed into system (6). Next, the characteristics of the equilibrium points and their eigenvalues are analyzed.

Set the parameters as $a_1 = 22, a_2 = 12, a_3 = 6, a_4 = 8$. Then, the equilibrium points and the corresponding eigenvalues of system (6) are displayed in Table 1. The distribution of those equilibrium points in x–y plane is shown in Fig. 1, in which the symbol '$\star$' represents the equilibrium points of system (6).

Table 1. The equilibrium points and eigenvalues of system (6).

Equilibrium points	Eigenvalues	Type
$S_1(-13.01,-0.54,264.0)$	$\lambda_{1,2}=2.29\pm12.19\mathrm{i}$, $\lambda_3=-20.54$	saddle-focus of index 2
$S_2(-0.54,13.01,264.0)$	$\lambda_{1,2}=2.29\pm12.19\mathrm{i}$, $\lambda_3=-20.54$	saddle-focus of index 2
$S_3(0.54,-13.01,264.0)$	$\lambda_{1,2}=2.29\pm12.19\mathrm{i}$, $\lambda_3=-20.54$	saddle-focus of index 2
$S_4(13.01,0.54,264.0)$	$\lambda_{1,2}=2.29\pm12.19\mathrm{i}$, $\lambda_3=-20.54$	saddle-focus of index 2

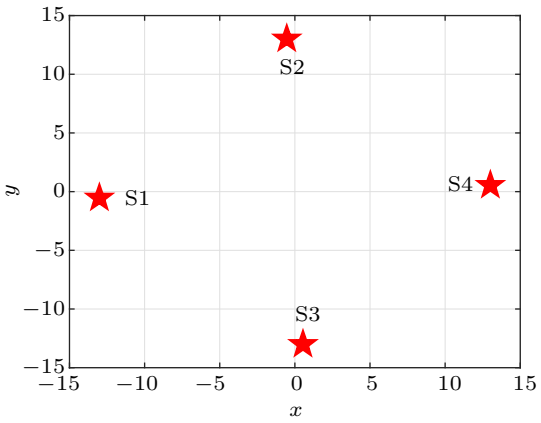


Fig. 1. Distribution of the equilibrium points of system (6).

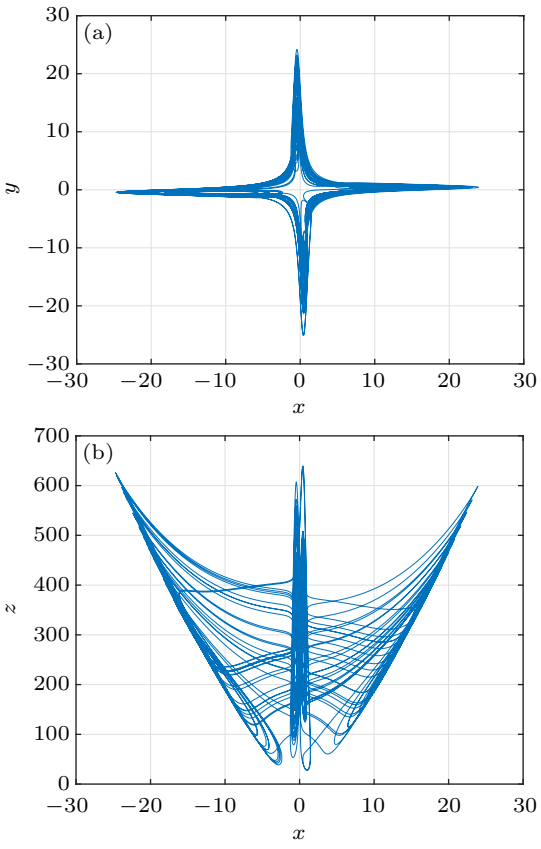


Fig. 2. The chaotic attractor of system (6): (a) x–y plane; (b) x–z plane.

It can be seen from Table 1 that system (6) has four saddle-focus equilibrium points of index 2. Thus, it can generate a 4-wing chaotic attractor. For given initial values $[x_0,y_0,z_0]^{\mathrm{T}}=[1,1,1]^{\mathrm{T}}$, the 4-wing chaotic attractor is shown in Fig. 2.

Meanwhile, the three Lyapunov exponents of system (6) are $LE1=1.2201$, $LE2=-0.0017$, and $LE3=-17.2275$. According to the formula $D_{\mathrm{L}}=2+(LE1+LE2)/|LE3|$, the Lyapunov dimension is $D_{\mathrm{L}}=2.0707$, which suggests that the attractor is fractional.[39]

3. A switched chaotic system based on a class of switching functions

Clearly, for system (6), there exists a one-to-one correspondence between the number of saddle-focus points and the number of wings. In this section, by constructing a class of switching functions, the number of saddle-focus equilibrium points with index 2 on both sides of the origin can be increased. It means that the number of wings of the chaotic attractors can be further expanded.

First, a switched system is proposed on the basis of the transformed system (6) by replacing the variable x in the right sides of Eq. (6) by T_x, which can be described by

$$\begin{bmatrix}\dot{x}\\ \dot{y}\\ \dot{z}\end{bmatrix}=\frac{1}{4T_x^2+4y^2}\begin{bmatrix}2T_x & 2y & 0\\ -2y & 2T_x & 0\\ 0 & 0 & 4T_x^2+4y^2\end{bmatrix}\times\begin{bmatrix}-a_1(T_x^2-y^2)+(2T_xy)z\\ -(T_x^2-y^2)+a_2(2T_xy)\\ -a_3z+a_4(2T_xy)^2\end{bmatrix},\tag{7}$$

in which T_x is a switching function of the state variable x, and also it is symmetric about the origin.

Given the initial value $[x_0,y_0,z_0]^{\mathrm{T}}=[1,1,1]^{\mathrm{T}}$ and keeping the values of a_1,a_2,a_3,a_4 unchanged, the switching function T_x is designed to adjust the distribution and the number of the saddle-focus equilibrium points. Thereby different kinds of multi-wing chaotic attractors can be generated. Here are the details.

Case 1: Take

$$T_x=\begin{cases}x+e, & x<0,\\ x-e, & x\geq 0.\end{cases}\tag{8}$$

Set the parameter $e=5$, the equilibrium points of system (7) with the switching function (8) are displayed in Table 2. The distribution of those equilibrium points in x–y plane is exhibited in Fig. 3, in which the symbol '$\circ$' represents the equilibrium points obtained in case 1 and '$\star$' denotes the equilibrium points of the original system (6). Obviously, the equilibrium points have been expanded from the previous four to six.

Thus, system (7) has six saddle-focus equilibrium points and therefore can generate a 6-wing chaotic attractor, which is shown in Fig. 4.

In case 1, the three Lyapunov exponents of the switched chaotic system are $LE1=1.8000$, $LE2=0.3210$, and $LE3=$

−18.1241. And, the Lyapunov dimension of the attractor is increased to 2.1170.

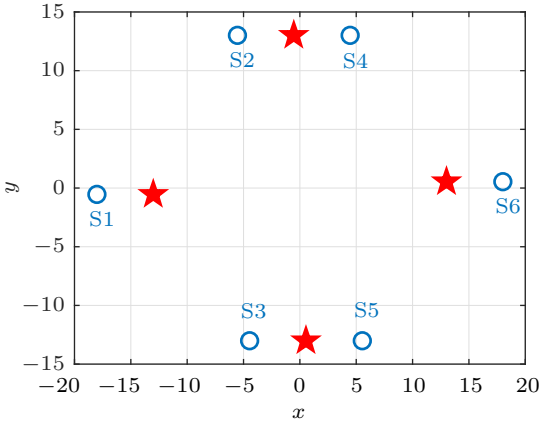


Fig. 3. Distribution of equilibrium points of system (7) in case 1.

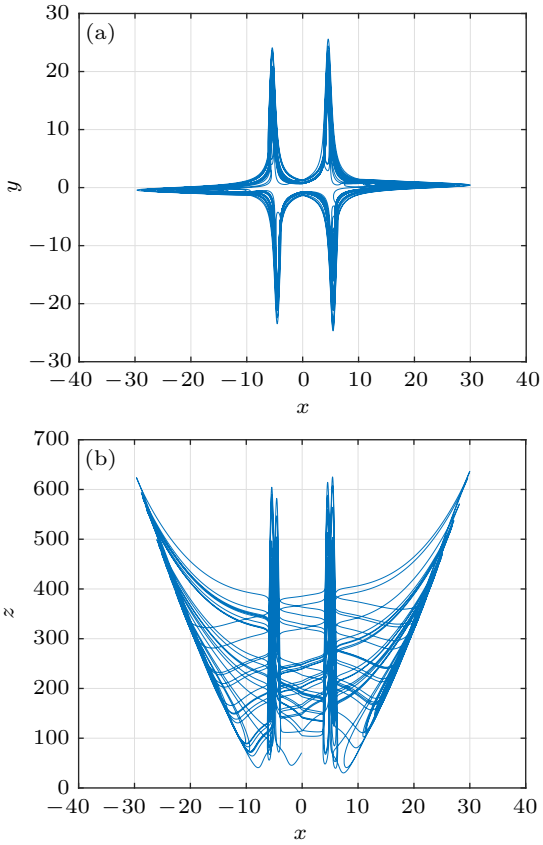


Fig. 4. The chaotic attractor of system (7) in case 1: (a) x–y plane; (b) x–z plane.

Case 2: Take

$$T_x = \begin{cases} x+2e, & x < -e, \\ x, & -e \le x < e, \\ x-2e, & x \ge e. \end{cases} \tag{9}$$

When designing the switching function T_x as Eq. (9), set the parameter $e = 5$, the equilibrium points of system (7) are displayed in Table 3. The distribution of these equilibrium points in x–y plane is presented in Fig. 5, in which the symbol '×' represents the equilibrium points in case 2 and '⋆' denotes the equilibrium points of the original system (6). From Fig. 5, we can see that the equilibrium points have been expanded from the previous four to eight.

Table 2. The equilibrium points and eigenvalues of system (7) in case 1.

Equilibrium points	Eigenvalues	Type
$S_1(-18.01,-0.54,264.0)$	$\lambda_{1,2} = 2.29 \pm 12.19\mathrm{i}$, $\lambda_3 = -20.54$	saddle-focus of index 2
$S_2(-5.54,13.01,264.0)$	$\lambda_{1,2} = 2.29 \pm 12.19\mathrm{i}$, $\lambda_3 = -20.54$	saddle-focus of index 2
$S_3(-4.46,-13.01,264.0)$	$\lambda_{1,2} = 2.29 \pm 12.19\mathrm{i}$, $\lambda_3 = -20.54$	saddle-focus of index 2
$S_4(4.46,13.01,264.0)$	$\lambda_{1,2} = 2.29 \pm 12.19\mathrm{i}$, $\lambda_3 = -20.54$	saddle-focus of index 2
$S_5(5.54,-13.01,264.0)$	$\lambda_{1,2} = 2.29 \pm 12.19\mathrm{i}$, $\lambda_3 = -20.54$	saddle-focus of index 2
$S_6(18.01,0.54,264.0)$	$\lambda_{1,2} = 2.29 \pm 12.19\mathrm{i}$, $\lambda_3 = -20.54$	saddle-focus of index 2

Table 3. The equilibrium points and eigenvalues of system (7) in case 2.

Equilibrium points	Eigenvalues	Type
$S_1(-23.01,-0.54,264.0)$	$\lambda_{1,2} = 2.29 \pm 12.19\mathrm{i}$, $\lambda_3 = -20.54$	saddle-focus of index 2
$S_2(-10.54,13.01,264.0)$	$\lambda_{1,2} = 2.29 \pm 12.19\mathrm{i}$, $\lambda_3 = -20.54$	saddle-focus of index 2
$S_3(-9.46,-13.01,264.0)$	$\lambda_{1,2} = 2.29 \pm 12.19\mathrm{i}$, $\lambda_3 = -20.54$	saddle-focus of index 2
$S_4(-0.54,13.01,264.0)$	$\lambda_{1,2} = 2.29 \pm 12.19\mathrm{i}$, $\lambda_3 = -20.54$	saddle-focus of index 2
$S_5(0.54,-13.01,264.0)$	$\lambda_{1,2} = 2.29 \pm 12.19\mathrm{i}$, $\lambda_3 = -20.54$	saddle-focus of index 2
$S_6(9.46,13.01,264.0)$	$\lambda_{1,2} = 2.29 \pm 12.19\mathrm{i}$, $\lambda_3 = -20.54$	saddle-focus of index 2
$S_7(10.54,-13.01,264.0)$	$\lambda_{1,2} = 2.29 \pm 12.19\mathrm{i}$, $\lambda_3 = -20.54$	saddle-focus of index 2
$S_8(23.01,0.54,264.0)$	$\lambda_{1,2} = 2.29 \pm 12.19\mathrm{i}$, $\lambda_3 = -20.54$	saddle-focus of index 2

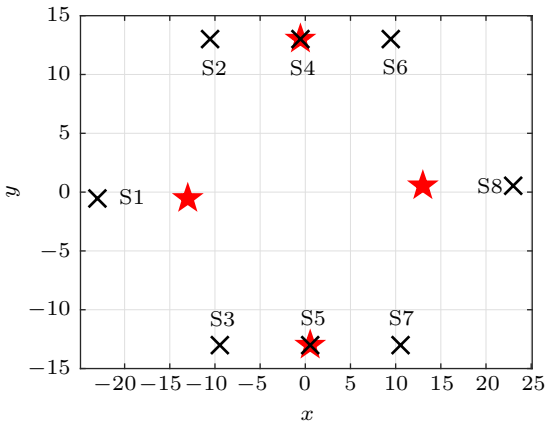


Fig. 5. Distribution of equilibrium points of system (7) in case 2.

In this case, system (7) has eight saddle-focus equilibrium points and therefore produces a 8-wing chaotic attractor, which is demonstrated in Fig. 6.

In case 2, the three Lyapunov exponents of the switched chaotic system are $LE1 = 2.8066$, $LE2 = -0.1807$, and $LE3 =$

−18.6331. Thus, the Lyapunov dimension of the attractor is increased to 2.1409.

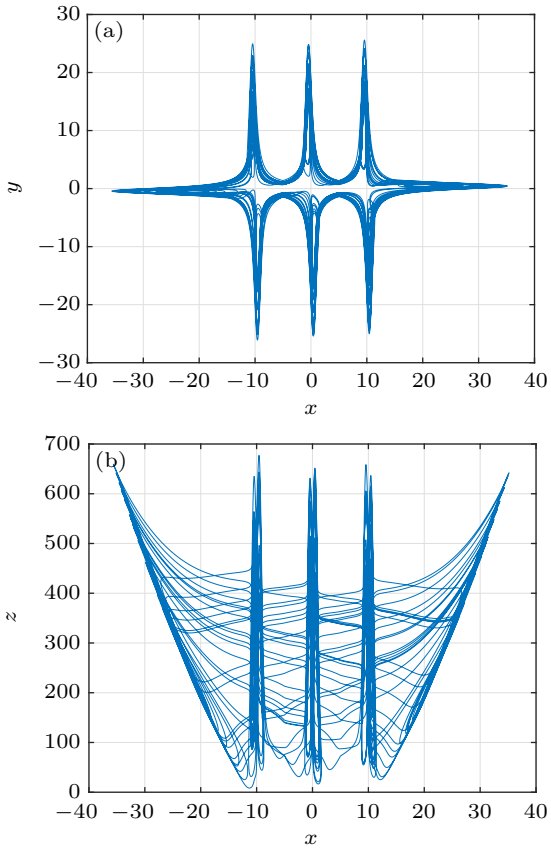


Fig. 6. The chaotic attractor of system (7) in case 2: (a) x–y plane; (b) x–z plane.

Case 3: Take

$$T_x = \begin{cases} x+4e, & x \le -3e, \\ x+2e, & -3e < x \le -e, \\ x, & -e < x \le e, \\ x-2e, & e < x \le 3e, \\ x-4e, & x > 3e. \end{cases} \tag{10}$$

Set the parameter $e = 5$, the equilibrium points and their eigenvalues of system (7) with the switching function (10) are shown in Table 4. The distribution of those equilibrium points in x–y plane is demonstrated in Fig. 7, in which the symbol '△' represents the equilibrium points in case 3 and '⋆' denotes the equilibrium points of the original system (6). Obviously, the equilibrium points have been expanded from the previous four to twelve.

Thus, in this case, system (7) has twelve saddle-focus equilibrium points and can generate a 12-wing chaotic attractor, which is demonstrated in Fig. 8.

In case 3, the three Lyapunov exponents are $LE1 = 4.0855$, $LE2 = -0.8212$, and $LE3 = -19.2708$, respectively. The Lyapunov dimension of the attractor is increased to 2.1694.

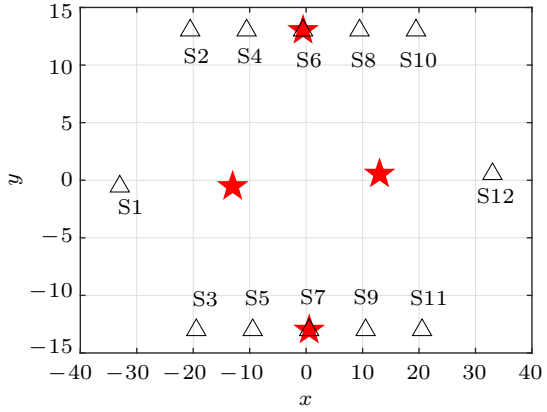


Fig. 7. Distribution of equilibrium points of system (7) in case 3.

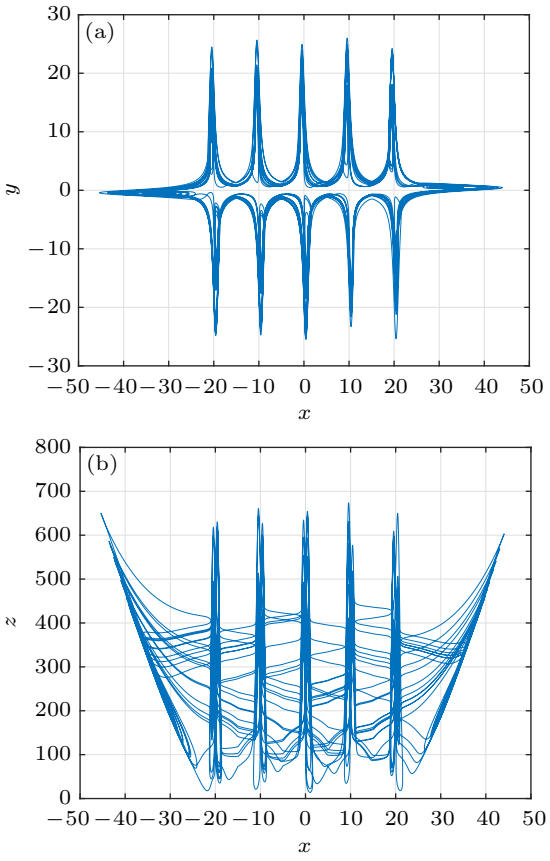


Fig. 8. The chaotic attractor of system (7) in case 3: (a) x–y plane; (b) x–z plane.

Case 4: Take

$$T_x = \begin{cases} x+6e, & x \le -5e, \\ x+4e, & -5e < x \le -3e, \\ x+2e, & -3e < x \le -e, \\ x, & -e < x \le e, \\ x-2e, & e < x \le 3e, \\ x-4e, & 3e < x \le 5e, \\ x-6e, & x > 5e. \end{cases} \tag{11}$$

Set the parameter $e = 5$, with the switching function (11), the equilibrium points and their eigenvalues of system (7) are displayed in Table 5. The distribution of those equilibrium points

in x–y plane is exhibited in Fig. 9, in which the symbol '□' represents the equilibrium points obtained in case 4 and '⋆' denotes the equilibrium points of the original system (6). Obviously, the equilibrium points have been expanded from the previous four to sixteen.

Thus, system (7) has sixteen saddle-focus equilibrium points and therefore can generate a 16-wing chaotic attractor, which is shown in Fig. 10.

In case 4, the three Lyapunov exponents are $LE1 = 4.5384$, $LE2 = -0.9897$, and $LE3 = -19.5547$, respectively. Therefore, the Lyapunov dimension of the attractor is increased to 2.1815.

Table 4. The equilibrium points and eigenvalues of system (7) in case 3.

Equilibrium points	Eigenvalues	Type
$S_1(-33.01,-0.54,264.0)$	$\lambda_{1,2}=2.29\pm12.19\mathrm{i}$, $\lambda_3=-20.54$	saddle focus of index 2
$S_2(-20.54,13.01,264.0)$	$\lambda_{1,2}=2.29\pm12.19\mathrm{i}$, $\lambda_3=-20.54$	saddle focus of index 2
$S_3(-19.46,-13.01,264.0)$	$\lambda_{1,2}=2.29\pm12.19\mathrm{i}$, $\lambda_3=-20.54$	saddle focus of index 2
$S_4(-10.54,13.01,264.0)$	$\lambda_{1,2}=2.29\pm12.19\mathrm{i}$, $\lambda_3=-20.54$	saddle focus of index 2
$S_5(-9.46,-13.01,264.0)$	$\lambda_{1,2}=2.29\pm12.19\mathrm{i}$, $\lambda_3=-20.54$	saddle focus of index 2
$S_6(-0.54,13.01,264.0)$	$\lambda_{1,2}=2.29\pm12.19\mathrm{i}$, $\lambda_3=-20.54$	saddle focus of index 2
$S_7(0.54,-13.01,264.0)$	$\lambda_{1,2}=2.29\pm12.19\mathrm{i}$, $\lambda_3=-20.54$	saddle focus of index 2
$S_8(9.46,13.01,264.0)$	$\lambda_{1,2}=2.29\pm12.19\mathrm{i}$, $\lambda_3=-20.54$	saddle focus of index 2
$S_9(10.54,-13.01,264.0)$	$\lambda_{1,2}=2.29\pm12.19\mathrm{i}$, $\lambda_3=-20.54$	saddle focus of index 2
$S_{10}(19.46,13.01,264.0)$	$\lambda_{1,2}=2.29\pm12.19\mathrm{i}$, $\lambda_3=-20.54$	saddle focus of index 2
$S_{11}(20.54,-13.01,264.0)$	$\lambda_{1,2}=2.29\pm12.19\mathrm{i}$, $\lambda_3=-20.54$	saddle focus of index 2
$S_{12}(33.01,0.54,264.0)$	$\lambda_{1,2}=2.29\pm12.19\mathrm{i}$, $\lambda_3=-20.54$	saddle focus of index 2

Table 5. The equilibrium points and eigenvalues of system (7) in case 4.

Equilibrium points	Eigenvalues	Type
$S_{1,16}(\mp43.01,\mp0.54,264.0)$	$\lambda_{1,2}=2.29\pm12.19\mathrm{i}$, $\lambda_3=-20.54$	saddle-focus of index 2
$S_{2,15}(\mp30.54,\pm13.01,264.0)$	$\lambda_{1,2}=2.29\pm12.19\mathrm{i}$, $\lambda_3=-20.54$	saddle-focus of index 2
$S_{3,14}(\mp29.46,\mp13.01,264.0)$	$\lambda_{1,2}=2.29\pm12.19\mathrm{i}$, $\lambda_3=-20.54$	saddle-focus of index 2
$S_{4,13}(\mp20.54,\pm13.01,264.0)$	$\lambda_{1,2}=2.29\pm12.19\mathrm{i}$, $\lambda_3=-20.54$	saddle-focus of index 2
$S_{5,12}(\mp19.46,\mp13.01,264.0)$	$\lambda_{1,2}=2.29\pm12.19\mathrm{i}$, $\lambda_3=-20.54$	saddle-focus of index 2
$S_{6,11}(\mp10.54,\pm13.01,264.0)$	$\lambda_{1,2}=2.29\pm12.19\mathrm{i}$, $\lambda_3=-20.54$	saddle-focus of index 2
$S_{7,10}(\mp9.46,\mp13.01,264.0)$	$\lambda_{1,2}=2.29\pm12.19\mathrm{i}$, $\lambda_3=-20.54$	saddle-focus of index 2
$S_{8,9}(\mp0.54,\pm13.01,264.0)$	$\lambda_{1,2}=2.29\pm12.19\mathrm{i}$, $\lambda_3=-20.54$	saddle-focus of index 2

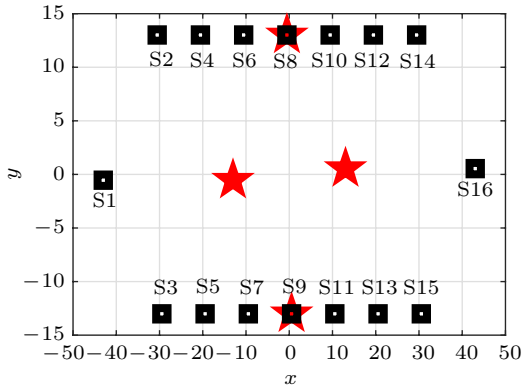


Fig. 9. Distribution of equilibrium points of system (7) in case 4.

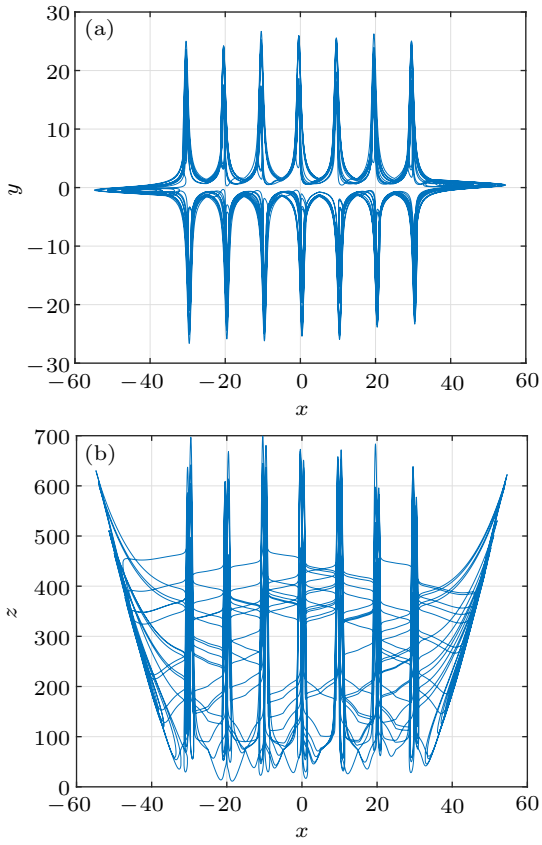


Fig. 10. The chaotic attractor of system (7) in case 4: (a) x–y plane; (b) x–z plane.

4. Dynamic analysis of the switched system

In this section, the complex dynamic behaviors of the switched system will be studied. By analyzing the Poincaré maps, the Lyapunov exponent spectra, and the bifurcation diagrams, some detailed dynamic properties for the switched system (7) will be revealed.

4.1. Poincaré maps

Fixing $a_1 = 22, a_2 = 12, a_3 = 6, a_4 = 8, e = 5$, and the initial value $[x_0, y_0, z_0]^{\mathrm{T}} = [1, 1, 1]^{\mathrm{T}}$, taking $z = 200$ as the crossing plane, the Poincaré maps of system (7) are displayed in Fig. 11. It can be seen from Figs. 11(a)–11(d) that the four

different Poincaré maps are consistent with the previously obtained 6-to-8-12-16-wing chaotic attractors, which verify the existence of the multi-wing chaotic attractors.

4.2. Lyapunov exponent spectra and bifurcation diagrams

Besides, taking the threshold parameter e as the bifurcation parameter and keeping the values of the other parameters unchanged, the Lyapunov exponent spectra and bifurcation diagrams of system (7) for the four cases are displayed in Figs. 12 and 13. Note that the parameter range for e is selected as $0 < e < 25$ in the simulations. From Figs. 12 and 13, it can be seen that system (7) is chaotic for a large range of parameter $1 < e < 25$. In addition, an interesting phenomenon can be observed, that is, the bifurcation diagrams consist of $2, 3, 5, 7$ branches, respectively, which are entirely consistent with the number of the segments in the switching functions.

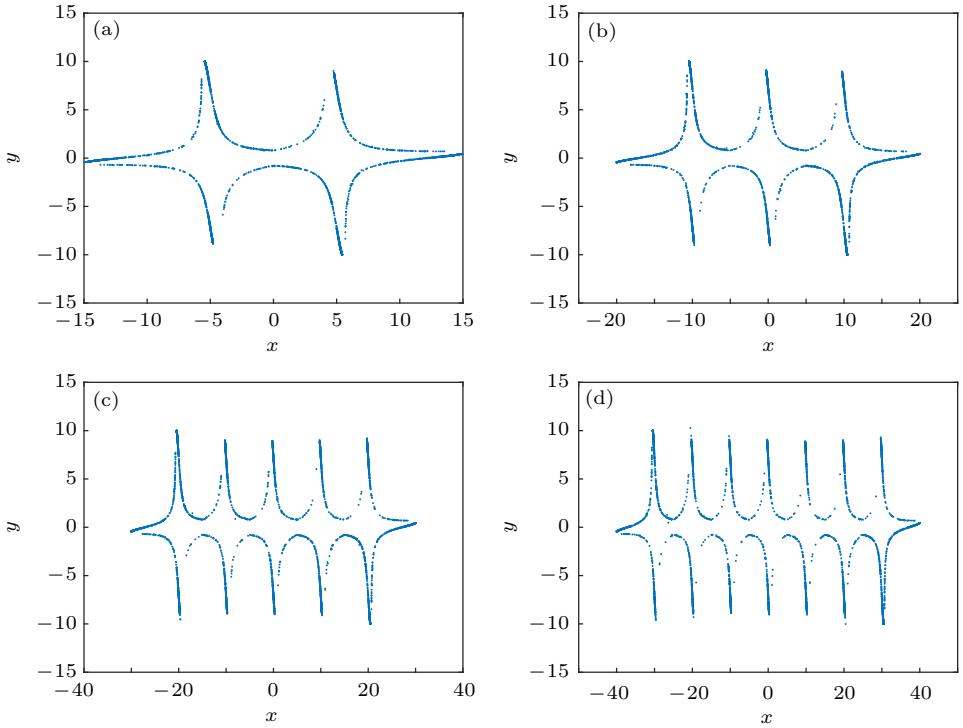


Fig. 11. Poincaré map on the cross-section $z = 200$: (a) case 1; (b) case 2; (c) case 3; (d) case 4.

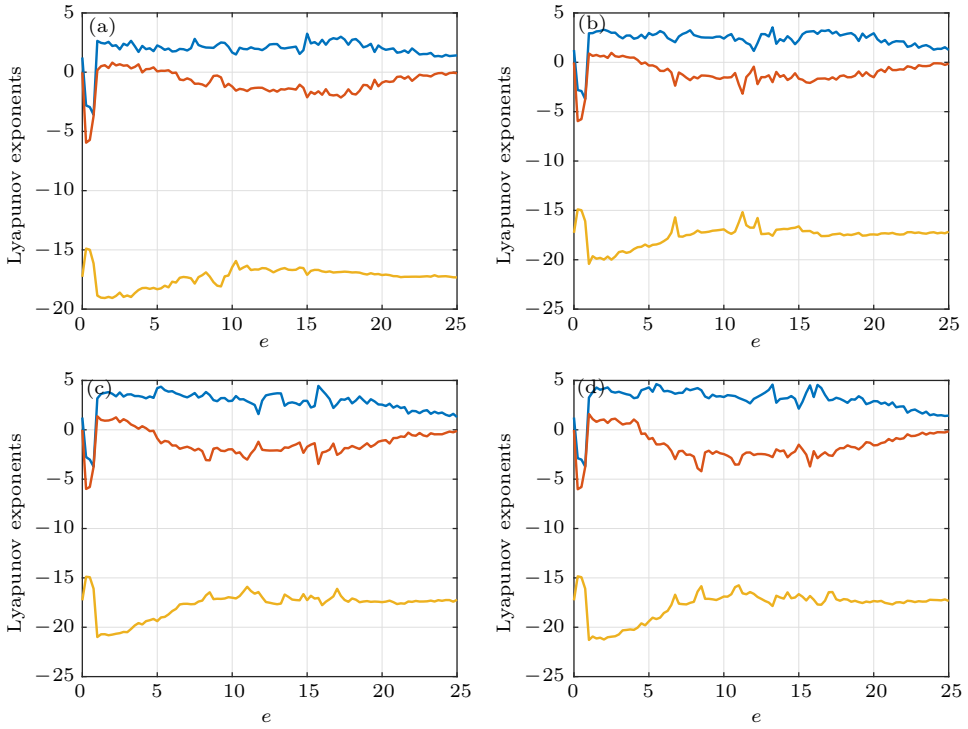


Fig. 12. Lyapunov exponent spectra of system (7): (a) case 1; (b) case 2; (c) case 3; (d) case 4.

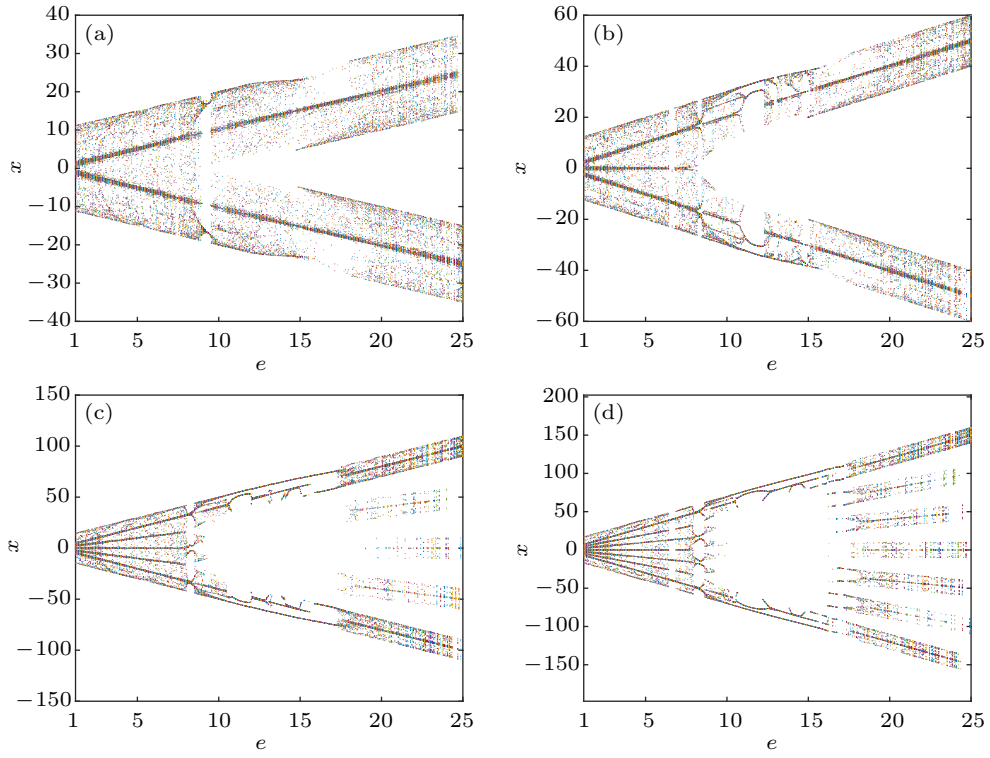


Fig. 13. Bifurcation diagrams of system (7) with respect to e: (a) case 1; (b) case 2; (c) case 3; (d) case 4.

5. FPGA implementation

In this section, the Verilog HDL code is designed for switched chaotic system (7). Meanwhile, the 6-to-8-12-16-wing chaotic attractors are implemented by FPGA. In particular, the improved Euler algorithm is used to describe the system first. Then, a three-stage state machine is employed to describe the whole iterative process. Finally, the output digital chaotic sequences are transmitted to DAC, and the phase diagrams of the chaotic attractors are observed from the oscilloscope.

Before designing the model for the system, the dynamic range of the variables should be considered first. In order to prevent the values of the variables from overflowing, we must compress the system first. The compression factors for variables x, y, z are respectively taken as $K_1 = 2^5, K_2 = 2^5, K_3 = 2^9$. Thus, the dimensionless state equation of system (7) is obtained as follows:

$$\begin{cases} \dot{x} = \dfrac{2T_x \times (-a_1(T_x^2 - y^2) + 2K_3 T_x yz) + 2y \times (-(T_x^2 - y^2) + 2a_2 T_x y)}{4T_x^2 + 4y^2}, \\ \dot{y} = \dfrac{-2y \times (-a_1(T_x^2 - y^2) + 2K_3 T_x yz) + 2T_x \times (-(T_x^2 - y^2) + 2a_2 T_x y)}{4T_x^2 + 4y^2}, \\ \dot{z} = -a_3 z + a_4 \times (2T_x y)^2 \times K_1^2 K_2^2 / K_3, \end{cases} \tag{12}$$

and notice that all the constant items and the switching threshold in T_x are reduced to $1/K_1$ of their original value. Taking case 2 as an example. When the system is compressed, T_x can be further rewritten as

$$T_x = \begin{cases} x + \dfrac{2e}{K_1}, & x < -\dfrac{e}{K_1}, \\ x, & -\dfrac{e}{K_1} \le x < \dfrac{e}{K_1}, \\ x - \dfrac{2e}{K_1}, & x \ge \dfrac{e}{K_1}. \end{cases} \tag{13}$$

Next, the k-step input vector of the system is denoted as $X_k = (x_k, y_k, z_k)^{\mathrm{T}}$, the right-side function of the state equation is marked as $F(X_k)$, and the step size of the iteration is set to $h = 1/128$. Then, the discretization equation of the chaotic system is obtained as

$$X_{k+1} = X_k + F[X_k + F(X_k) \times 0.5h] \times h.$$

First of all, we use 24-bit fixed-point numbers to describe the variables of the system. In these 24-bit binary numbers, we use 18 of them to represent decimals. Then, the three-stage state machine of the system is designed. The so-called three-stage state machine uses three always modules. Among them, the first always module uses synchronous timing to describe

the state transition. The second always module uses combinational logic to judge the state transition conditions and to describe the state transition rules. The third always module describes the state output. By using the state machine, the jump of the iteration operation can be easily realized, and each step of the iteration can be described in different state processes. The design of the state machine for the system is shown in Fig. 14.

In S0 state, the switching function T_x can be realized by the selection output process of the multiplexer. Following the state jump process, the addition, subtraction, multiplication and division operations in the iterative process can be implemented by the status bits S1 to S20. Thus, in S21 state, we get $X_{k+0.5}$ or X_{k+1} of the k-step iteration. If jump_position = 0, then output $X_{k+0.5}$, and the state machine jumps to the S0 state to perform another round of calculation; if jump_position = 1, then output X_{k+1}, X_{k+1} is the output vector of the k-step iterative operation, which corresponds to the output of the chaotic sequence of the system. In S22 state, we add a 24-bit positive number to X_{k+1} to ensure that the input values to the DAC module are all positive. Finally, because the DAC module is 14 bits, it implies that we should intercept [21:8] bits of data as the final output.

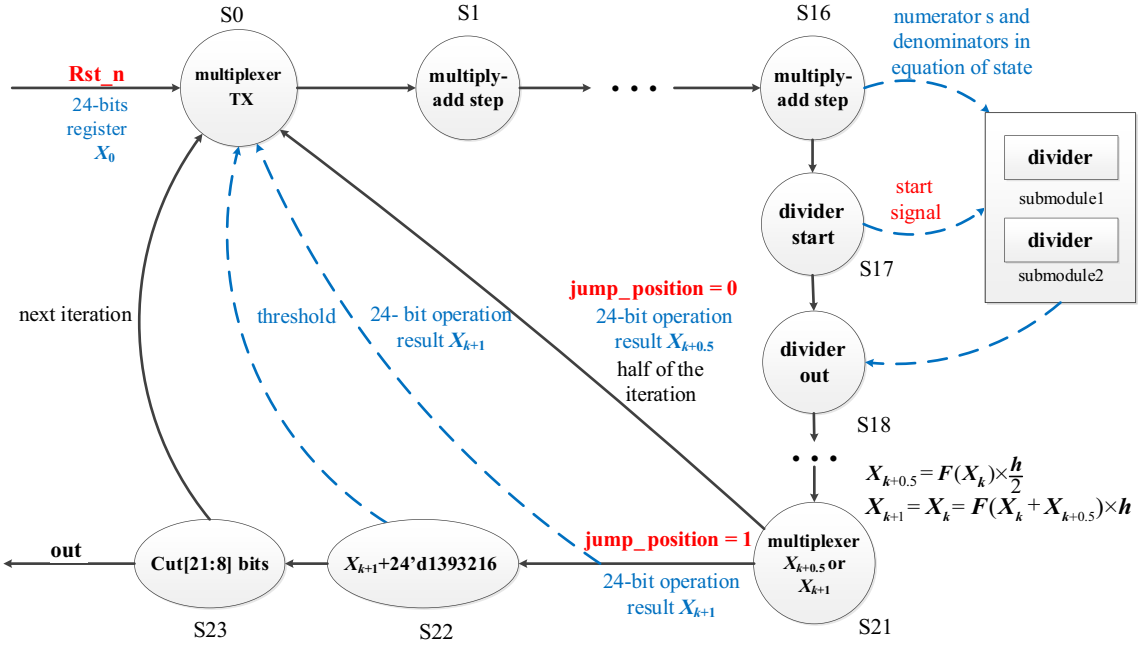


Fig. 14. State machine description of the system.

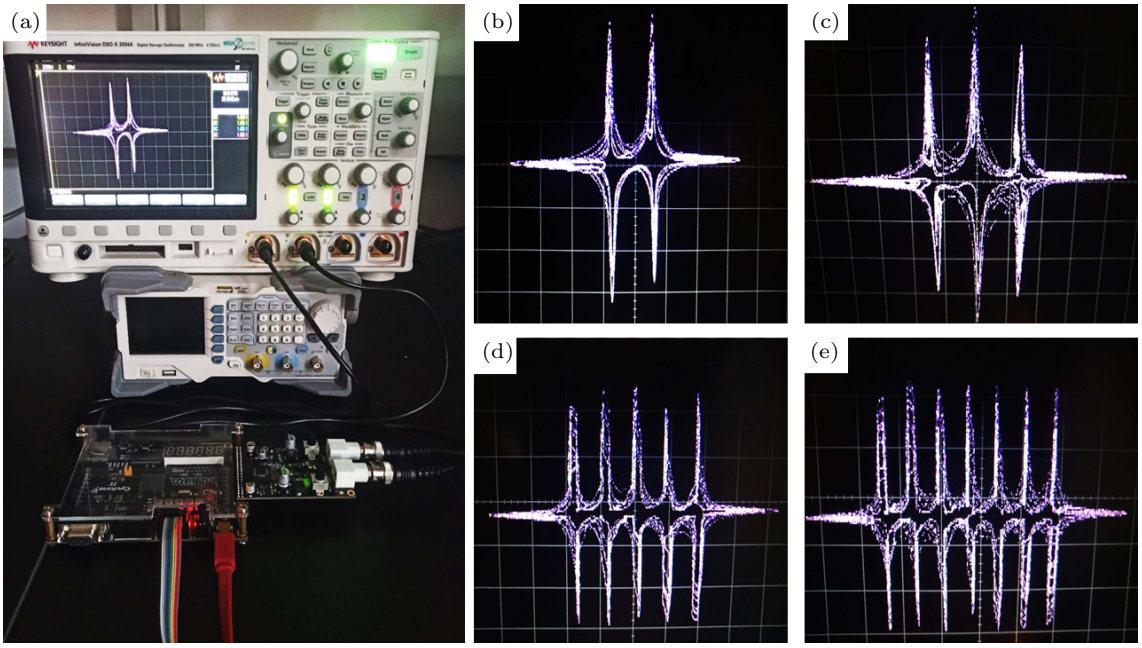


Fig. 15. Wiring diagram and phase diagrams of the generated chaotic attractors: (a) wiring diagram between AX301 and oscilloscope; (b) 6-wing attractor in case 1; (c) 8-wing attractor in case 2; (d) 12-wing attractor in case 3; (e) 16-wing attractor in case 4.

Thereafter, we compile the Verilog HDL code in Quartus II software and download it to the FPGA development board after synthesis. The FPGA development board that we use is AX301 board of Alinx, and the board carries Altera Cyclone IV EP4CE10F17C8 chip. Moreover, the development board is also equipped with a 14-bit DAC module AN9767, which can convert the digital chaotic sequence generated in the FPGA chip into analog voltage signals for output. Wiring diagram between AX301 and oscilloscope is shown in Fig. 15(a), and the observed phase diagrams of the 6-to-8-12-16-wing chaotic attractors are displayed in Figs. 15(b)–15(e), which confirm the existence of the chaotic attractors.

6. Conclusion

In this study, a multi-wing chaotic switched system with complicated topological structures is proposed on the basis of a 2-wing chaotic attractor via a combined method, and meanwhile the multi-wing chaotic attractors are realized by FPGA. In brief, the core of the design method is the combination of a quadratic transformation and a switching function. By the means of Lyapunov exponent spectra, bifurcation diagrams and Poincaré map analysis, some interesting dynamical phenomena are revealed. Besides, in the FPGA digital circuit design, Verilog HDL hardware description language is used to describe the system, and each step of the iterative operation is realized in the designed state machine. The observation of the multi-wing chaotic attractors on the oscilloscope verifies the validity of the proposed design method.

References

[1] Tsafack N, Kengne J, Abd-El-Atty B, Iliyasu A M, Hirota K and Abd El-Latif A A 2020 *Inf. Sci.* **515** 191
[2] Atangana A and Qureshi S 2019 *Chaos Solitons Fractals* **123** 320
[3] Khan J S and Ahmad J 2019 *Multidimens. Syst. Signal Process.* **30** 943
[4] Zhang C X and Yu S M 2013 *Int. J. Circuit Theory Appl.* **41** 221
[5] Yu S M, Lü J H, Chen G R and Yu X H 2010 *IEEE Trans. Circuits Syst. II-Express Briefs* **57** 803
[6] Ding P F, Feng X Y and Wu C M 2020 *Chin. Phys. B* **29** 108202
[7] Zhang G T and Wang F Q 2018 *Chin. Phys. B* **27** 018201
[8] Luo X H, Tu Z W, Liu X R, Cai C, Liang Y L and Gong P 2010 *Chin. Phys. B* **19** 070510
[9] Miranda R and Stone E 1993 *Phys. Lett. A* **178** 105
[10] Xiong L, Zhang S, Zeng Y C and Liu B Q 2018 *Chin. J. Phys.* **56** 2381
[11] Hu X Y, Liu C X, Liu L, Yao Y P and Zheng G C 2017 *Chin. Phys. B* **26** 110502
[12] He S B, Sun K H and Zhu C X 2013 *Chin. Phys. B* **22** 050506
[13] Yu F, Wang C H, Yin J W and Xu H 2011 *Chin. Phys. B* **20** 110505
[14] Ji Y and Bi Q S 2010 *Acta Phys. Sin.* **59** 7612 (in Chinese)
[15] Li C, Min F H, Jin Q S and Ma H Y 2017 *AIP Adv.* **7** 125204
[16] Peng Z P, Wang C H, Lin Y and Luo X W 2014 *Acta Phys. Sin.* **63** 240506 (in Chinese)
[17] Hua Z Y, Zhou Y C and Huang H J 2019 *Inf. Sci.* **480** 403
[18] Zhang L M, Sun K H, Liu W H and He S B 2017 *Chin. Phys. B* **26** 100504
[19] Li Y, Li Z J, Ma M L and Wang M J 2020 *Multimed. Tools Appl.* **79** 29161
[20] Huang L L, Zhang Z F, Xiang J H and Wang S M 2019 *Complexity* **2019** 5803506
[21] Zhang C X and Yu S M 2016 *Chin. Phys. B* **25** 050503
[22] Chang H, Li Y X and Chen G R 2020 *Chaos* **30** 043110
[23] Zhong X Y, Peng M F and Shahidehpour M 2019 *Int. J. Circuit Theory Appl.* **47** 686
[24] Zhang X and Wang C H 2019 *Int. J. Bifurcation Chaos* **29** 1950117
[25] Bao B C, Jiang T, Wang G Y, Jin P P, Bao H and Chen M 2017 *Nonlinear Dyn.* **89** 1157
[26] Xue W, Qi G Y, Mu J J, Jia H Y and Guo Y L 2013 *Chin. Phys. B* **22** 080504
[27] Huang Y 2014 *Acta Phys. Sin.* **63** 080505 (in Chinese)
[28] Luo M W, Luo X H and Li H Q 2013 *Acta Phys. Sin.* **62** 020512 (in Chinese)
[29] Zhou X, Wang C H and Guo X R 2012 *Acta Phys. Sin.* **61** 200506 (in Chinese)
[30] Qiu M, Yu S M, Wen Y Q, Lü J H, He J B and Lin Z S 2017 *Int. J. Bifurcation Chaos* **27** 1750040
[31] Wang F Q and Xiao Y F 2020 *Complexity* **2020** 9169242
[32] Liu Q, Fang J Q, Zhao G and Li Y 2012 *Acta Phys. Sin.* **61** 130508 (in Chinese)
[33] Wang H J, Song B B, Liu Q, Pan J and Ding Q 2014 *Int. J. Bifurcation Chaos* **24** 1450054
[34] Dong E Z, Yuan M F, Zhang C, Tong J G, Chen Z Q and Du S Z 2018 *Int. J. Bifurcation Chaos* **28** 1850081
[35] Shah D K, Chaurasiya R B, Vyawahare V A, Pichhode K and Patil M D 2017 *AEU-Int. J. Electron. Commun.* **78** 245
[36] Senouci A, Bouhedjeur H, Tourche K and Boukabou A 2017 *AEU-Int. J. Electron. Commun.* **82** 211
[37] Zhang C X, Yu S M and Zhang Y 2011 *Int. J. Mod. Phys. B* **25** 2183
[38] Yu S M, Tang W K S, Lü J H and Chen G R 2010 *Int. J. Circuit Theory Appl.* **38** 243
[39] Sprott J C 2011 *Int. J. Bifurcation Chaos* **21** 2391